29th Congress of the International Council of the Aeronautical Sciences
St. Petersburg, Russia; September 7-12, 2014

WIND TUNNEL INVESTIGATION OF CRITICAL FLIGHT REGIMES USING DYNAMICALLY SCALED ACTIVELY CONTROLLED MODEL IN 3 DOF GIMBAL

I. Grishin, A. Khrabrov, A. Kolinko, M. Sidoryuk, A. Vyalkov
Central Aerohydrodynamic Institute (TsAGI)

Keywords: *wind tunnel experiment, 3DOF Gimbal, controller design and validation*

Abstract

Possibility of wind tunnel research of aircraft dynamics at high angles of attack by means of an actively controlled scaled model on three-degree-of-freedom gimbal (pitch, roll and yaw) is justified. Results of mathematical simulation of self-induced oscillations on the gimbal and in the free flight are compared. The influence of friction in the gimbal on the modeling results is studied, as well as the model center of gravity shift relative to the gimbal reference point. Robust control design to suppress wing-rock type oscillations is outlined and modeling results are given.

Experimental open- and closed-loop control results obtained at the rig for single and two degrees of freedom configurations are presented.

1 Introduction

The study of flight dynamics at high angles of attack requires a mathematical model of unsteady aerodynamic characteristics, which is traditionally developed based on the results of experimental investigations of static and dynamic tests in wind tunnel (WT) using the forced oscillations rigs in pitch, roll and yaw. The problems of flight dynamics at high angles of attack are highly non-linear due to the flow separation. Therefore, the study of unsteady aerodynamics in wind tunnel should be carried out with the model moving as close as possible to the natural movement of the controlled aircraft. From this point of view, it is of great interest to perform experimental study of the free model oscillations, which are dynamically similar to those observed in flight.

For the experimental approximation of the natural unsteady flight motion of the aircraft, it is possible to use three-degree-of-freedom gimbal and actively controlled dynamically scaled aerodynamic model.

There have been several attempts to design control laws for aircraft using actively controlled models 'flying' in multiple degrees of freedom in wind tunnels. Single degree-of-freedom (DOF) rigs with actuated control surfaces were used for investigation of stability and control in [1-8]. A 2DOF rig (roll and yaw) using active control surfaces augmented with compressed-air blowing was developed and successfully used for testing H_∞ - control laws in [9]. Three and more degree of freedom rigs were developed and used in [10-13] to extract aerodynamic models, develop control systems and perform wind tunnel simulations of dynamic motions.

A full 6 DOF free flight setup was developed by NASA for the large-scale wind tunnel [14]. The tested model is free flying within the tunnel working section, with electrical power, compressed air and control signals from outside controllers and using three operators providing command control inputs on three channels. The cost of this type of setup is very high.

A 5 DOF pilot rig was developed and tested for a few degrees of freedom at the University of Bristol [11-12]. In [12] the ventral sting perpendicular to the flow of WT was used. It has been shown that using the dynamically

scaled controlled model mounted on the three-degrees-of-freedom gimbal in the wind tunnel allows obtaining an efficient and cost-effective study of aircraft static and dynamic stability derivatives and investigation of stability and control. However, this kinematic scheme allows study of unsteady aerodynamic characteristics only in a limited range of small and medium angles of attack. Limitations of kinematics due to the ventral sting do not allow investigation of the process of stalling, and especially the spin motion.

In the present work the use of the dorsal sting located along the wind tunnel flow velocity is proposed. Thus many of the restrictions associated with the ventral holder can be removed. The proposed 3-DOF rig allows investigation of large angles of attack phenomena, such as longitudinal pitching limit-cycle oscillations, or lateral–directional phenomena, such as wing rock and departure to spin.

2 Mathematical Model of a Controlled Model in 3 DOF Gimbal

A schematic view of a dynamic rig in WT (sting located along the velocity of the flow) is shown in Fig. 1.

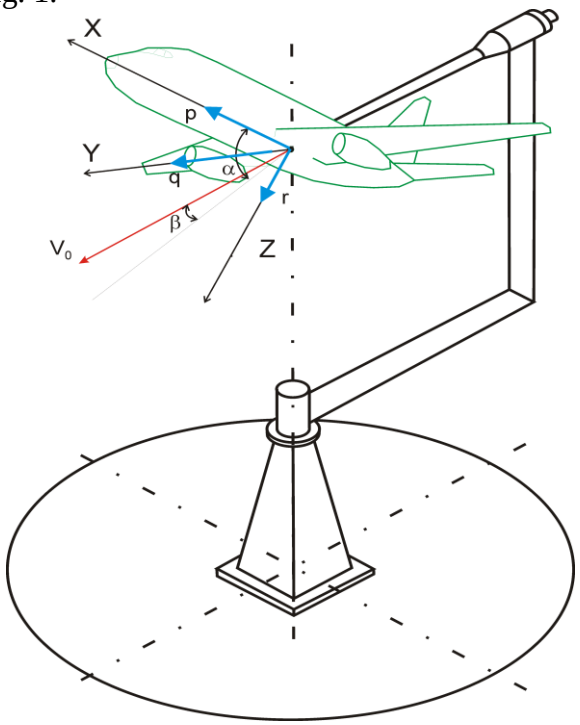

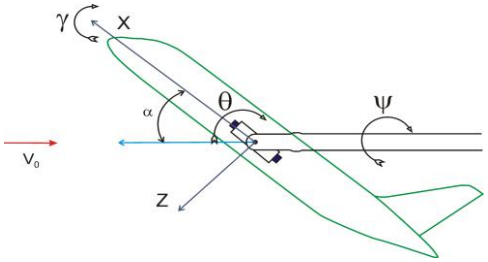

Fig.1. A scheme of three-degree-of-freedom dynamic rig in WT.

Position of the aircraft model in the 3DOF gimbal is defined by three Euler angles ψ,θ,γ. Yaw angle ψ lies in the range [-180, 180] degrees. The dorsal holder allows pitch angle θ vary inside the interval [20, 120] degrees, and roll angle vary in the range [-40, 40] degrees. The dynamics of the aircraft model in the 3DOF gimbal is described by the following system of differential equations:

$$\begin{aligned}
&\dot{\theta} = -r\sin\gamma + q\cos\gamma,\\
&\dot{\psi} = (r\cos\gamma + q\sin\gamma)/\sin\theta\\
&\dot{\gamma} = p - (r\cos\gamma + q\sin\gamma)/\tan\theta\\
&\dot{\omega} = J^{-1}(-\omega\times J\omega + M_a(\alpha,\beta,\omega,\delta)\\
&\qquad + M_g + M_f)
\end{aligned} \qquad (1)$$

where $\omega=(p,q,r)^T$ is a vector of body-axis angular velocity components of the model, $\delta=(\delta_e,\Delta\delta_e,\delta_a,\delta_r)^T$ is a control vector consisting on elevator δ_e,, differential elevator $\Delta\delta_e$,, aileron δ_a, and rudder surface δ_r deflections. M_a, M_g, and M_f are aerodynamic, gravity, and gimbal friction forces moments, respectively. Angle of attack α and sideslip angle β are defined by the following relations:

$$\begin{aligned}
&tg\alpha = tg\theta\cos\gamma,\\
&\sin\beta = \sin\theta\sin\gamma.
\end{aligned}$$

Body-axis components of non-dimensional aerodynamic moment have the following form:

$$\begin{aligned}
&C_m = C_{m0}(\alpha,\delta_e) + C_{mq}(\alpha)q\\
&C_l = C_{l\beta}(\alpha,\beta) + C_{lp}(\alpha)p + C_{lr}(\alpha)r + C_{l\delta_a}(\alpha,\delta_a)\\
&\qquad + C_{l\delta_r}(\alpha,\delta_r) + \Delta C_l(\alpha,\delta_e,\Delta\delta_e)\\
&C_n = C_{n\beta}(\alpha,\beta) + C_{np}(\alpha)p + C_{nr}(\alpha)r + C_{n\delta_a}(\alpha,\delta_a)\\
&\qquad + C_{n\delta_r}(\alpha,\delta_e,\delta_r) + \Delta C_n(\alpha,\delta_e,\Delta\delta_e).
\end{aligned} \qquad (2)$$

Gravity moment is caused by impossibility of ideal coincidence of the aircraft model center of gravity and gimbal center. Body-axis components M_{gx}, M_{gy}, M_{gz} of gravity moment M_g are the following (center of gravity discrepancy along y-axis is neglected):

$$M_{gx} = mg\Delta z_{c.g.}(\sin\psi\cos\gamma + \cos\psi\cos\theta\sin\gamma)$$
$$M_{gy} = -mg\Delta x_{c.g.}\cos\psi\cos\theta\cos\gamma + mg\Delta z_{c.g.}\cos\psi\sin\theta$$
$$M_{gz} = mg\Delta x_{c.g.}(\sin\psi\cos\gamma + \cos\psi\cos\theta\sin\gamma).$$

Friction moment in each axis of rotation (ψ,θ,γ) is modeled as a sum of dry and viscous friction with some coefficients to be identified:

$$\begin{aligned} Q_{f\psi} &= -k_{1\psi}\operatorname{sign}\dot{\psi} - k_{2\psi}\dot{\psi} \\ Q_{f\theta} &= -k_{1\theta}\operatorname{sign}\dot{\theta} - k_{2\theta}\dot{\theta} \\ Q_{f\gamma} &= -k_{1\gamma}\operatorname{sign}\dot{\gamma} - k_{2\gamma}\dot{\gamma}. \end{aligned} \qquad (3)$$

Body-axis components M_{fx}, M_{fy}, M_{fz} of friction moment M_f are as follows:

$$M_{fx} = Q_{f\gamma}$$
$$M_{fy} = Q_{f\theta}\cos\gamma - (Q_{f\gamma}\cos\theta - Q_{f\psi})\sin\gamma/\sin\theta$$
$$M_{fz} = -Q_{f\theta}\sin\gamma - (Q_{f\gamma}\cos\theta - Q_{f\psi})\cos\gamma/\sin\theta.$$

3 Comparison of Aircraft Motion in 3DOF Gimbal and in Free Flight

To justify a possibility of research in wind tunnel the aircraft dynamics at high angles of attack by means of a controlled scaled model on the 3DOF gimbal, a comparison of mathematical modeling of its dynamics with mathematical modeling of dynamics of the same model in flight is performed. In this comparison friction in gimbal and center of gravity displacement are neglected. The calculations were executed for available mathematical model of maneuverable aircraft.

3.1 Comparison of Attainable Equilibrium Sets

Important aircraft's performance and maneuvering capabilities in steady flight conditions are usually analyzed considering the steady states of the rigid-body equations of motion. Analysis of spatial aircraft maneuvers with intensive rotation is usually performed using a 5th order system of equations with respect to variables (α,β,p,q,r), describing short-period longitudinal and lateral aircraft motion. Steady-state spatial maneuvers are described by the stationary solutions of this system at different control surfaces deflections. Steady maneuver can be characterized by three parameters: angle of attack, sideslip angle and steady turning rate Ω. An important characteristic of the aircraft dynamics is the set of attainable maneuvers, i.e. achievable using available maximum δ_e, δ_a, δ_r control deflections. In [15] a procedure of reconstruction of attainable equilibrium sets and their local stability maps was proposed. Such maps provide a comprehensive and consistent representation of the aircraft flight and maneuvering envelopes.

It is interesting to compare attainable equilibrium sets for a model on 3 DOF gimbal and in free flight. To represent multidimensional set of all equilibrium states two-dimensional cross sections are computed for different fixed values of the other flight regime and maneuver parameters. These cross sections, or attainable equilibrium sets, are computed on a square grid of points. The grid points with attainable steady-state parameters are displayed using different markers reflecting their local stability properties. The calculation results are presented in the form of two-dimensional cross-sections in planes (α, β) and (α,Ω).

Stable steady states are marked by solid circles, whereas for unstable steady states, several different markers are used to reflect topology of the local dynamics:

1) Aperiodically unstable equilibria with one positive real eigenvalue are marked by x.
2) Oscillatory unstable equilibria with unstable complex conjugate pair of eigenvalues, are marked by ○.

In Fig. 2 an example of the calculated attainable equilibrium set cross-sections (α,β) and (α,Ω) is shown. It can be seen that the regions for the 3DOF gimbal and the free flight motion are very similar to each other.

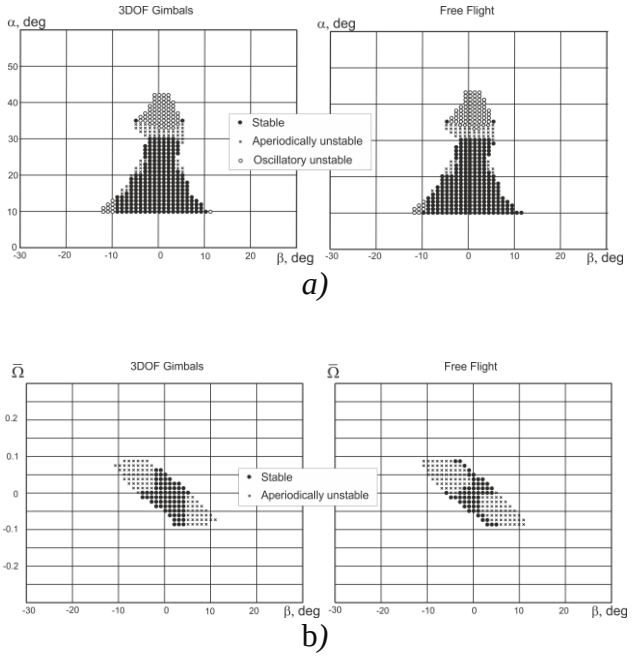

Fig.2. Comparison of attainable equilibrium sets for velocity-vector roll maneuver cross sections at a) Ω=0, b) α =20 deg.

Table 1 compares the eigenvalues of the aircraft model near the free horizontal flight, and the symmetrical position in the 3DOF gimbal. It can be seen that the eigenvalues, as well as elevator trim values are close to each other.

Table 1

Parameter	Model in 3DOF gimbal	Free model, 5th order equations
α_{trim}, deg	35	35
$\delta_{e\ trim}$, deg	-19.7410	-17.8947
Eigenvalues	$0.2282 \pm 0.5911i$ $-0.4072 \pm 0.6654i$ $-2.111, \quad 0$	$0.2682 \pm 0.5687i$ $-0.4025 \pm 0.5740i$ -2.187

3.2 Comparison of Self-Induced Oscillations

Another important comparison of the aircraft dynamics in the 3 DOF gimbal and in the free flight motion is performed comparing the lateral-directional self-induced oscillations at high angles of attack known as wing rock. Results of numerical simulation of the wing rock motion in the 3 DOF gimbal in WT and in the free flight motion described by full spatial aircraft motion equations are presented in Fig. 3. It can be seen that amplitudes of self-induced oscillations in angles of attack and sideslip, as well as angular rates, are rather close. Oscillation frequencies are also close. Amplitudes of roll oscillation are different.

Integrally, numerical simulation shows that the aircraft model on the 3 DOF gimbal in WT fairly models important features of the free flight.

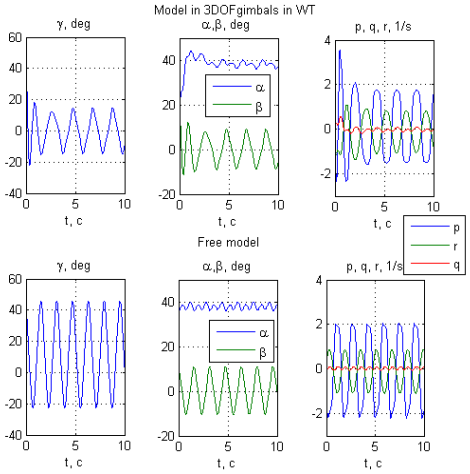

Fig.3. Comparison of wing rock oscillations in the 3 DOF gimbal in WT and in the free flight motion.

4 Influence of Friction and Center of Gravity Displacement

To identify the coefficients of dry $k_{1\theta}$, $k_{1\gamma}$, $k_{1\psi}$ and viscous $k_{2\theta}$, $k_{2\gamma}$, $k_{2\psi}$ friction and displacement of the center of gravity relative to the center of the gimbal, special experiments were made. Free oscillations of the aircraft model without flow for each of the axis of gimbal, as well as oscillations on a spring suspension were recorded. Approximation of the experimental records and numerical simulation results of the corresponding motions with the same initial conditions were compared,

minimizing one of the following target functions:

$$F_1 = \left\| \theta_{exper}(t) - \theta_{simul}(t, k_{1\theta}, k_{2\theta}, \Delta x_{c.g.}, \Delta z_{c.g.}) \right\| \quad (4)$$

for pitch motion,

$$F_2 = \left\| \gamma_{exper}(t) - \gamma_{simul}(t, k_{1\gamma}, k_{2\gamma}, \Delta x_{c.g.}, \Delta z_{c.g.}) \right\| \quad (5)$$

for roll motion, and

$$F_3 = \left\| \psi_{exper}(t) - \psi_{simul}(t, k_{1\psi}, k_{2\psi}, \Delta x_{c.g.}, \Delta z_{c.g.}) \right\| \quad (6)$$

for yaw motion, respectively.

The objective function (4) (5), or (6) were calculated on some grid by linear interpolation of the experimental results and the results of mathematical modeling, and minimized considering values of $k_{1\theta}$, $k_{2\theta}$, (or $k_{1\gamma}$, $k_{2\theta}$, $k_{1\psi}$, $k_{2\psi}$), and $\Delta x_{c.g.}$, $\Delta z_{c.g.}$ as parameters. Optimization tools of MATLAB were used. Results of optimization are presented in Figs. 4-6. In the result of minimization procedures the following parameter values were found:

$k_{1\theta}$=0.04, $k_{2\theta}$=0.07, $k_{1\psi}$=0.0005,
$k_{2\psi}$=0.0026, $k_{1\gamma}$=0.005, $k_{2\gamma}$=0.01,
$\Delta x_{c.g.}$=-0.0016(m), $\Delta z_{c.g}$ =0.0031(m).

Figures 7-9 show the simulation results of the perturbed motion, including self-oscillations of the aircraft model in the 3DOF gimbal in WT at high angles of attack with the identified values of the model center of gravity displacement relative to the center of the gimbal and friction parameters for several values of elevator deflection. For comparison, dotted lines show the similar transients in the absence of friction and displacement of the center of gravity. It can be seen that influence of friction and non-ideal centers coincidence is not significant. Flow velocity of WT in simulations was taken equal to 25 m/s.

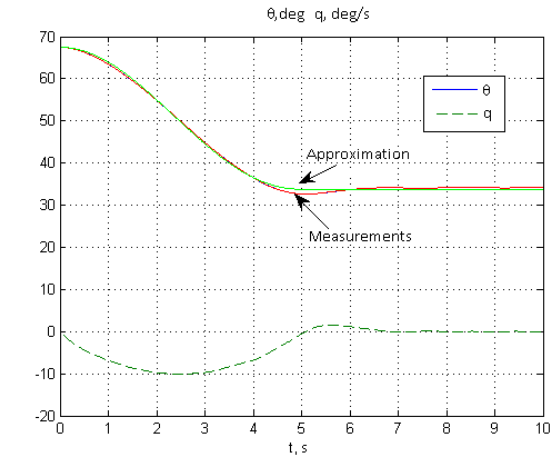

Fig.4. Fitting of experimental data: pitch free oscillation.

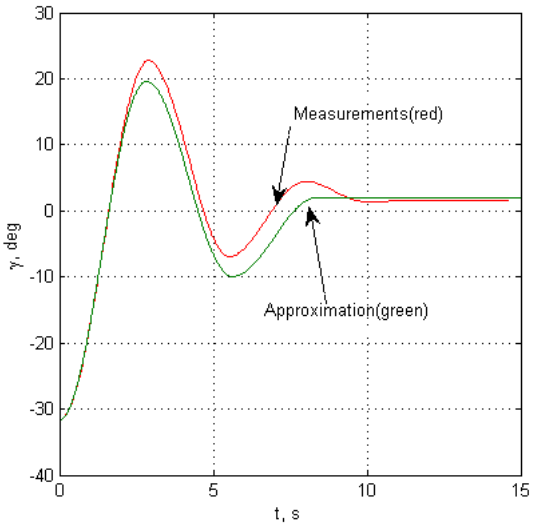

Fig.5. Fitting of experimental data: roll free oscillation

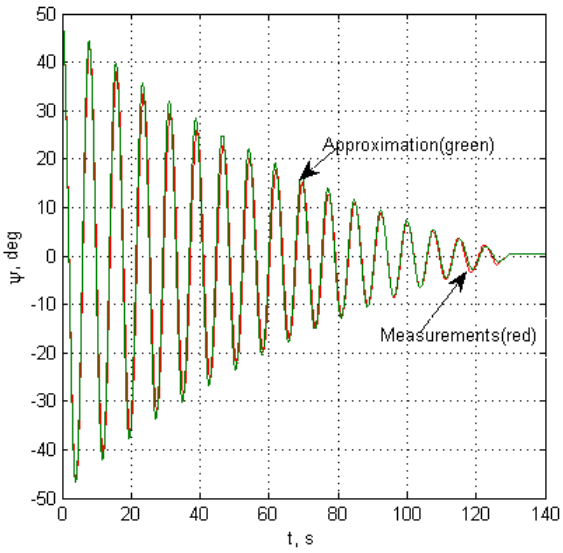

Fig.6. Fitting of experimental data: yaw oscillations in spring suspension.

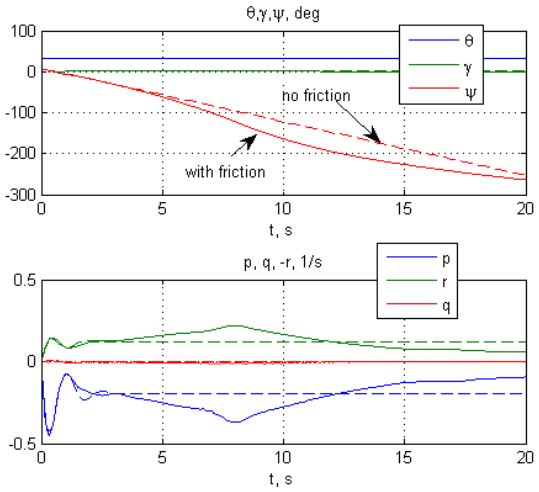

Fig. 7. Simulation of aircraft model response in 3 DOF gimbal, δ_e=-22 deg.

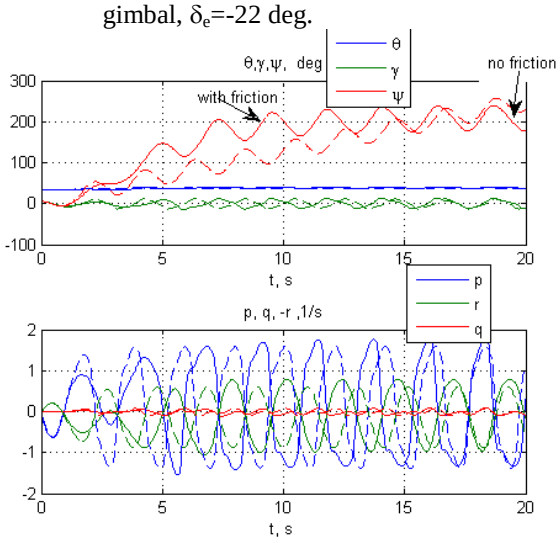

Fig. 8. Simulation of self-induced oscillations of aircraft model in 3 DOF gimbal, δ_e=-23 deg.

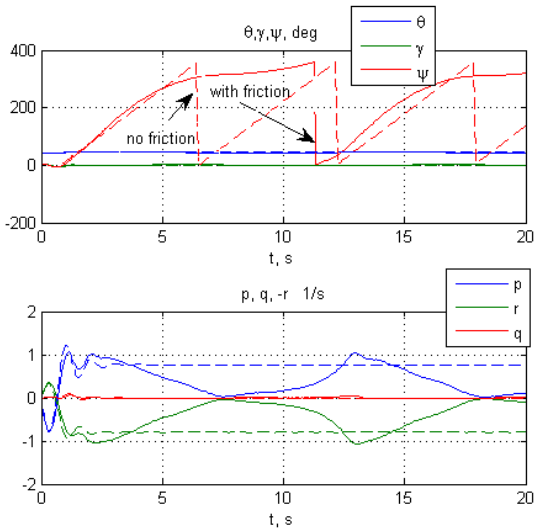

Fig. 9. Simulation of aircraft model in 3 DOF gimbal response, δ_e=-27 deg.

4 Control law design

To suppress large amplitude oscillations of aircraft model on the 3DOF gimbal in WT at angles of attack α>35deg and improve stability properties at smaller angles of attack, robust control laws were designed. To improve longitudinal stability, a simple pitch damper is used to produce the following control input on elevator deflection:

$$\delta_e = \delta_{e\,trim} + K_q q \qquad (7)$$

To improve lateral/directional stability and suppress wing-rock type oscillations, two different control laws for differential elevator as a control effector were designed. The first one is a simple proportional control law:

$$\Delta\delta_e = K_\gamma \gamma + K_\psi \psi + K_p p + K_r r \qquad (8)$$

The control law gains were calculated using the pole placement in LMI regions approach [16, 17]. This approach allows obtaining robust controllers for a certain range of parameters of parameter dependent plants. The design goal was to stabilize lateral/directional motion for a certain range of angles of attack, providing pole placement in the intersection of the half-plane x<-0.3 and of the conic sector centered at the origin and with inner angle 3π/4.

Another control law was designed using the Linear Parameter Varying (LPV) approach for quasi-linear control plants, similar to the approach used for the aircraft wing rock suppression in [18]. To construct a control law that suppresses the wing rock motion at high angles of attack, such a simplification of the nonlinear lateral-directional equations is considered in which oscillations near the symmetric aircraft model position still remain:

$$\begin{aligned}
\dot{\gamma} &= p - r / \tan\theta_0 \\
\dot{\psi} &= p + \tan\theta_0 r \\
\dot{p} &= \Delta L(\theta_0, \beta(\theta_0, \gamma)) + L_p p + L_r r + L_{\Delta\delta_e}\Delta\delta_e \\
\dot{r} &= N_\beta \beta + N_p p + N_r r + N_{\Delta\delta_e}\Delta\delta_e .
\end{aligned} \qquad (9)$$

System (9) has a single non-linearity $\Delta L(\theta_0, \beta(\theta_0, \gamma))$. The following parameter is introduced:

$$\rho(\gamma(t)) = \begin{cases} \dfrac{\Delta L(\theta_0, \gamma(t))}{\gamma}, & \gamma \neq 0 \\ 0, & \gamma = 0 \end{cases}$$

This allows reducing system (9) to the LPV form and applying gain-scheduled H_∞ control techniques for LPV systems [19-20]. As a result, a 4th order linear parameter dependent control law of the following form was obtained:

$$\dot{x}_K = A_K(\rho(t))x_K + B_K(\rho(t))y$$
$$u = C_K(\rho(t))x_K + D_K(\rho(t))y.$$

Here $y = (\gamma \ \psi \ p \ r)^T$ is the control measurement vector, and x_k is the vector of controller inner variables. Gains of this controller depend on the amplitude of the perturbed oscillations.

Nonlinear simulation taking into account the first order actuator model 1/(0.011s+1), time delay due to the control real-time implementation up to 0.05s, and the available aerodynamic model (2), approves both design approaches for providing lateral-directional stability. An example of the closed-loop system numerical simulation with the designed LPV controller is shown in Fig. 10.

An objective point is an experimental validation of both control laws and getting an experience in tuning control design parameters depending on the specific features of the real-time control implementation. This work is not done yet. The following section presents the experimental results obtained up to the present.

5 Experimental Studies

The model being used for the wind tunnel rig is an approximate 1/14 scale of real aircraft. Its mass is about 4.5 kg. It has a conventional set of control surfaces driven by model aircraft servos. The aircraft model is controlled via a wireless link, which also serves for data transfer.

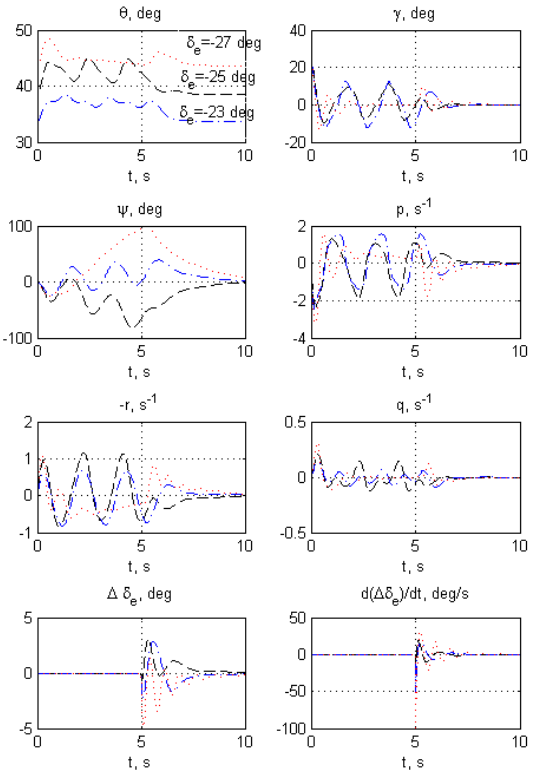

Fig. 10. Wing rock developing and suppression switching on the control law at t=5s.

3-DOF gimbal is used to achieve rotation in three degrees of freedom: pitch, roll, and yaw. Except 3DOF motion, the facility provides any single-DOF configuration and any 2DOF motion combination. The attitude of the model in gimbal is measured by three high resolution optical encoders (accuracy $\pm 0.07^o$). An inertial measurement unit supplied by Kalman filter is used also. Angular velocities are measured by gyros placed inside the model with accuracy $\pm 0.025^o$/s. Data acquisition is performed at frequency 100Hz, and control is performed at 50Hz. The wind tunnel experiments were performed at flow speed 25 m/s. A wind tunnel flow turbulence level is approximately 3%.

5.1 1 DOF Experimental Results

The typical open loop experimental results for the 1DOF pitch-only case are presented in Fig. 11. Measured pitch angle θ, pitch rate q and input control surface deflection δ_{elev} (left

and right) are shown. During step-wise elevator deflection from -12deg to -24deg the model gradually changes the trim pitch angle. In the range of elevator deflection of $-30° < \delta_{elev} < -24°$ self-induced pitch oscillations arise.

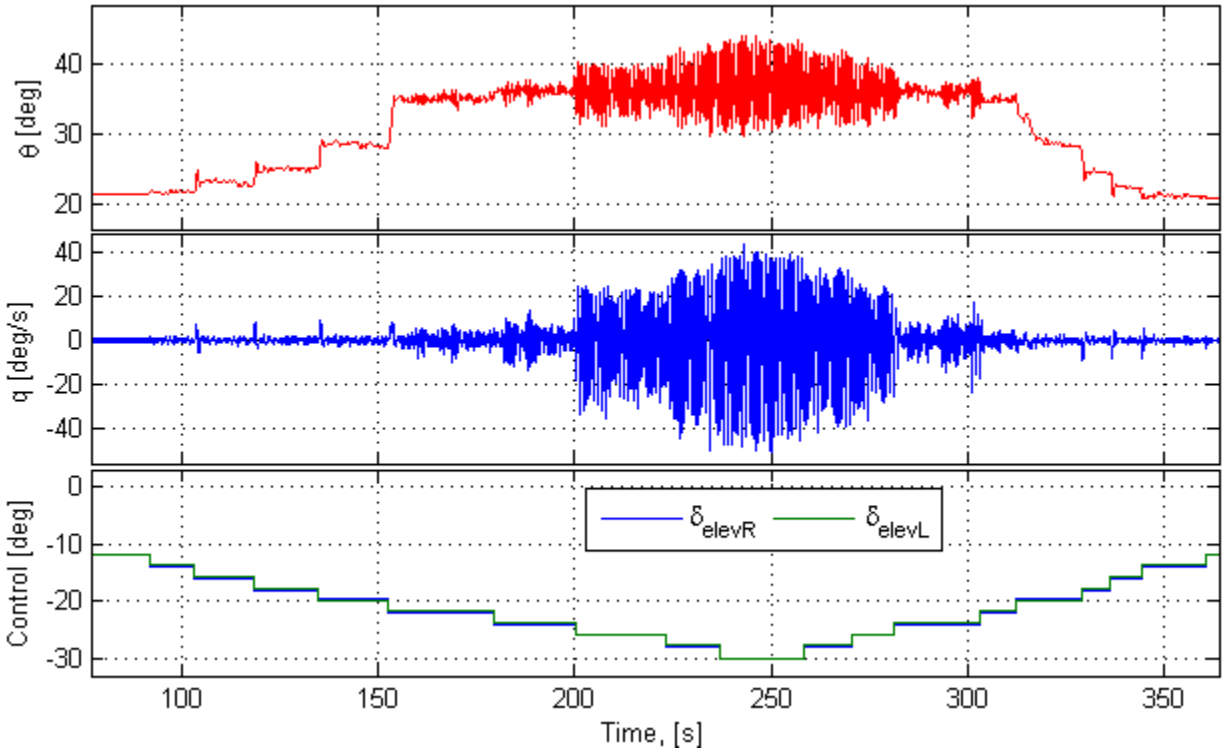

Fig. 11. Open-loop 1 DOF pitch experiment.

To suppress self-induced pitch oscillations, the pitch damper (7) with a varying control gain was used. An example of oscillation's suppression with the gain K_q=0.1 is shown in Fig. 12. The control system is switched on during the time from t=210 s till t=225 s and then it is switched off. The results show that the control system effectively reduces the amplitude of self-induced pitch oscillations from 10° to $1.5 \div 2°$. Residual oscillations are due to wind tunnel turbulence.

5.2 2 DOF Experimental Results

Two cases of couple degree of freedom configuration were investigated:

- 2 DOF pitch-roll case
- 2 DOF pitch-yaw case

The typical open loop experimental results for the 2 DOF pitch-roll case are presented in Fig. 13. Measured output pitch angle θ, roll angle γ, roll rate p pitch rate q and control input deflection δ_{elev} are shown. Step-wise elevator deflection $-20° < \delta_{elev} < -12°$ gradually changes

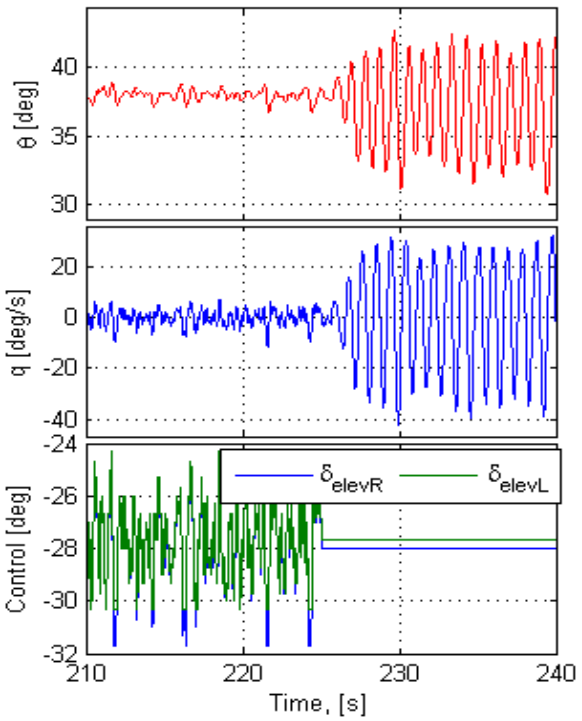

Fig. 12. Closed-loop 1 DOF pitch experiment.

the model trim pitch angle. An abrupt jump of pitch trim angle was observed at $\delta_{elev} = -20°$. In the range of elevator deflection $-24° < \delta_{elev} < -20°$ self-induced roll oscillations arise. In the range $-30° < \delta_{elev} < -24°$ the model motion is unstable both in roll and pitch. Self-induced oscillations of large amplitude are observed.

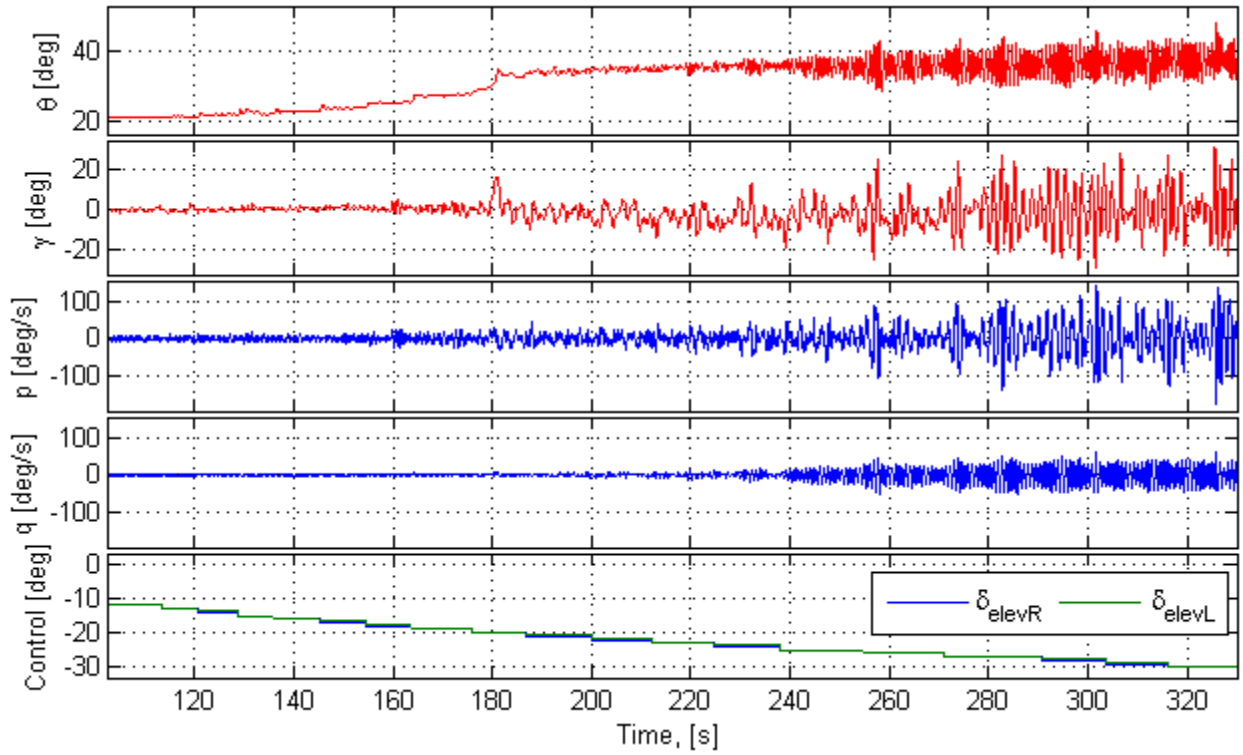

Fig. 13. Open-loop 2 DOF pitch-roll experiment.

To suppress pitch-roll self-induced oscillations, the control law (7)-(8) was used. The following gains were selected: $K_\psi = 0$, $K_r = 0$, $K_q = 0.10$, $K_p = -0.09$, $K_\gamma = 0.15$. An example of pitch-roll oscillation's suppression is shown in Fig. 14. The control system is switched on from t=200 s till t=220 s and then switched off. The results of study show that the control system effectively reduces the amplitude of self-induced pitch oscillations from $7 \div 8°$ to $1.5 \div 2°$ and roll oscillations from $24°$ to $7 \div 8°$.

An example of 2 DOF pitch and yaw oscillations suppression is shown in Fig. 16. The appropriate gains of the control law (7) - (8) are the following: $K_\psi = 0.40$, $K_r = -0.09$, $K_q = 0.30$, $K_p = 0$, $K_\gamma = 0$. The control system is on at $t = 510 \div 530$ s and $t = 545 \div 560$ s. The control system decreases longitudinal oscillations from $7 \div 8°$ to $1.5 \div 2°$ and stabilizes yaw angle.

5.3 3 DOF Open-Loop Experimental Results

The typical 3 DOF open loop experimental results are presented in Fig. 16. During step-wise elevator deflection the lateral stability of the model is lost in the range $-30° < \delta_{elev} < -20°$. The model is rotating at high yawing rate. Attempts to stabilize the 3 DOF motion were not successful as yet.

6 Conclusions and Further Work

The use of an actively controlled wind tunnel model mounted on a purposely designed, three degree-of-freedom gimbal support, have shown an ability to provide investigation of critical flight regimes at high angles of attack. Friction in the gimbal has been estimated and found insignificant for high angles of attack phenomena study. Control laws for longitudinal

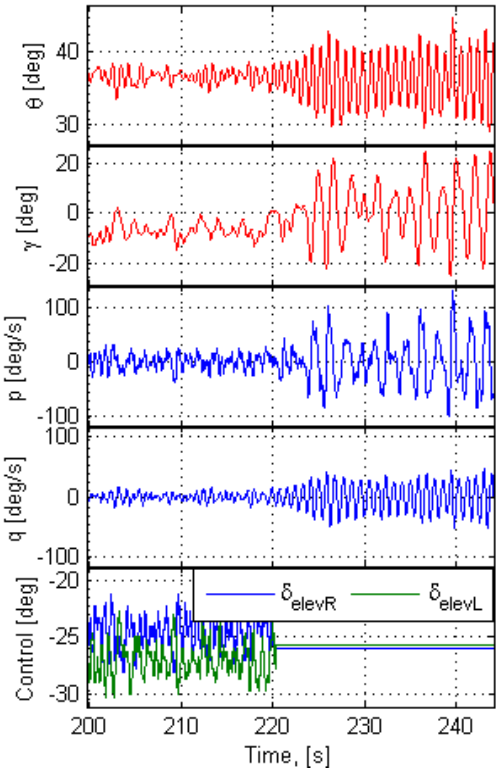

Fig. 14. Closed loop 2 DOF pitch-roll experiment.

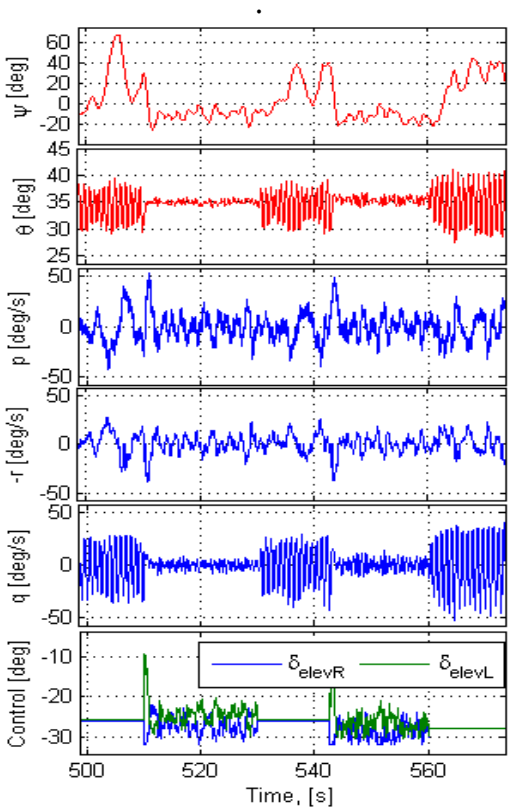

Fig. 15. Closed loop 2 DOF pitch-yaw experiment.

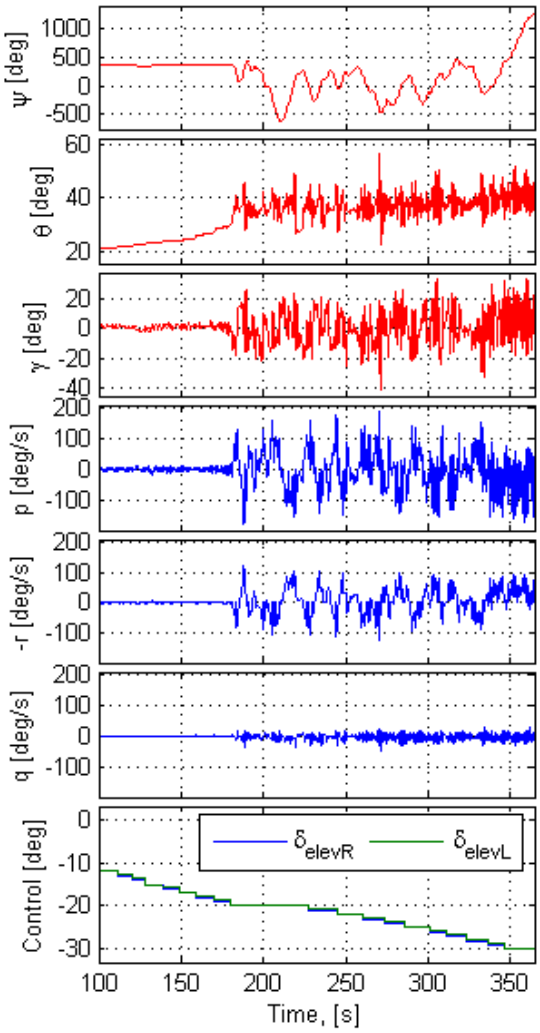

Fig. 16. Open loop 3 DOF experiment.

and lateral-directional stability augmentation and wing rock suppression were proposed. 1 DOF and 2 DOF open-loop and closed-loop experiments demonstrate promising results.

While carrying out the experimental work the use of the rig for control law validation has been demonstrated, however, some problems and limitations have been also identified.

One such problem is the absence of adequate aerodynamic model. Additional experiments for aerodynamic moments measurements were conducted to introduce clarity into the available mathematical model. These experiments development were executed using the same rig equipped with the internal strain-gage balance. Besides, some aerodynamic model parameters were identified from open-loop step maneuvers. Current experimental technique limitations are the following: a

relatively high time delay in radio-controlled model servos, a relatively high wind tunnel turbulence level, a low control sampling rate, and some others.

A further work supposes overcoming some of the mentioned problems and carrying out the 3DOF experiments with different control laws.

Acknowledgements

This work is partially supported by the Russian Foundation for Basic Research (no. 12-08-00679).

References

[1] Capone F.J, Owens D.B, Hall R.M. Development of a transonic free-to-roll test capability. *Journal of Aircraft*, Vol. 41, No.3, 2004.

[2] Rajamurthy M.S. Generation of comprehensive longitudinal aerodynamic data using dynamic wind tunnel simulation. *Journal of Aircraft*, Vol. 34, No. 1, 1997.

[3] Bennet R.M, Farmer M.G, Mohr R.L, Hall W.E. Wind-tunnel technique for determining stability derivatives from cable-mounted models. *Journal of Aircraft*, Vol. 15, No. 5, 1978.

[4] Magill J.C, Cataldi P, Morency J.R, Hammer D.X, Anderson B.D. Design of a wire suspension system for dynamic testing in AEDC 16T. *AIAA Paper 2003-452, 41st Aerospace Science Meeting and Exhibit*, 6-9 January 2003, Reno, Nevada, USA.

[5] Khrabrov A, Zhuk A. Using of large amplitude free oscillations in pitch and roll to investigate unsteady aerodynamic characteristics at separated flow regimes. *ICIASF'95 Record*. - Ohio, USA, pp 241-247, July 18-21, 1995.

[6] Cook, M. V. On the use of small scale aircraft models for dynamic wind tunnel investigation of stability and control. *Trans. of the Institute of Measurement and Control*, Vol. 9, No. 4, pp. 190–197, 1987.

[7] Davison P.M, di Bernardo M., and Lowenberg M.H., Modelling and control of a single degree-of-freedom dynamic wind tunnel rig. *European Control Conference* 2003 (ECC2003), Univ. of Cambridge, UK, Sept. 2003.

[8] Davison P, Lowenberg M.H, di Bernardo M. Experimental analysis and modeling of limit cycles in a dynamic wind-tunnel rig. *J. of Aircraft*. V. 40, N. 4, pp 777-785, 2003.

[9] Papageorgiou G, Glover K. Design, development and control of the HIRM wind tunnel model. *European Conference on Decision and Control*, Dec. 1999.

[10] Davison P, Lowenberg M.H, di Bernardo M. Experimental analysis and modeling of limit cycles in a dynamic wind-tunnel rig. *J. of Aircraft*. V. 40, N. 4, pp 777-785, 2003.

[11] Gatto A, Lowenberg M.H. Evaluation of a three-degree-of-freedom test rig for stability derivative estimation. *J. of Aircraft*. V. 43, N. 6, pp 1747-1762, 2006.

[12] Pattinson J, Lowenberg M, Goman M. A Multi-degree-of-freedom rig for the wind tunnel determination of dynamic data. *AIAA Atmospheric Flight Mechanics Conference*, Chicago, USA, 10-13 August, 2009, AIAA Paper 2009-5727.

[13] A. Sen, N. Bhange, P. Wahi, A. Ghosh, 5-Degree-of-freedom dynamic rig for wind tunnel tests of aerospace vehicles. *AIAA Atmospheric Flight Mechanics Conference*, Chicago, USA, AIAA Paper 2009-5605, Aug, 2009.

[14] Chambers, J.R. Modeling flight: the role of dynamically scaled free-flight models in support of NASA's aerospace programs. NASA SP 2009-575.

[15] Goman M.G, Khramtsovsky A, and Kolesnikov E. Evaluation of aircraft performance and maneuverability by computation of attainable equilibrium sets, *Journal of Guidance, Control, and Dynamics*, Vol. 31, No. 2, pp 329-339, 2008.

[16] Chilary M., Gahinet P. H_∞ Design with pole placement constraints: an LMI approach. *IEEE Transactions on Automatic Control*. V. 40, 1995.

[17] Gahinet P, Nemirovsky A, Laub A, Chilary M. *Robust control toolbox*. The Math Works Inc.

[18] Sidoryuk M. LPV control design to suppress wing rock motion. *5th European conference for aerospace sciences (EUCASS)*, Munich, 2-7 July 2013.

[19] Apkarian P, Gahinet P. A convex characterization of gain-scheduled H_∞ controllers. *IEEE Transactions on Automatic Control*, V.40, No.5, 1995.

[20] Apkarian P, Gahinet P, Becker G. Self-scheduled H_∞ control of linear parameter-varying systems: a design example. *Automatica*, V. 31, pp.1251-1261, 1995.

7 Contact Author Email Address

mailto: msid@mail.ru

Copyright Statement